Rocznik Ochrona Środowiska

Volume 27 Year 2025 ISSN 2720-7501 pp. 82-95

https://doi.org/10.54740/ros.2025.008 open access

Received: September 2024 Accepted: February 2025 Published: February 2025

Energy Dissipation in High-Performance Concrete under Repeated Compressive Loading

Asif Iqbal. A. Momin[1], Rajesab B. Khadiranaikar[2], Abdullah Naser M. Asiri[3], Tinku Biswas[4], Md Anzar Rabbani[5], Aijaz Ahmad Zende[1], Vedprakash Maralapalle[6], Saiful Islam[3]*

[1]*Department of Civil Engineering, BLDEA's Vachana Pitamaha Dr. P.G Halakatti College of Engineering and Technology, Vijayapur, Affiliated to VTU, Belagavi, Karnataka, India*

[2]*Department of Civil Engineering, SECAB Institute of Engineering and Technology, Vijayapur, Affiliated to VTU, Belagavi, Karnataka, India*

[3]*Civil Engineering Department, College of Engineering, King Khalid University, Abha, Saudi Arabia*

[4]*Deputy Manager, Central quality assurance, DLF Ltd, Gurgaon, India*

[5]*Ganga Institute of Technology and Management, Bahadurgarh-Jhajjar Road Kablana Jhajjar, Haryana, India*

[6]*Department of Civil Engineering, Amity School of Engineering and Technology, Amity University Maharashtra, Mumbai – Pune Expressway, Bhatan Post – Somathne, Panvel, Mumbai, Maharashtra, India*

[*]*corresponding author's e-mail: aijaz.52964@gmail.com*

Abstract: This study focuses on the energy dissipation characteristics of High-Performance Concrete (HPC) under uniaxial repeated compressive loading for three different grades. The objective is to analyze the energy dissipation capacity of HPC by examining the stress-strain hysteresis during repeated loading. The dimensionless energy dissipation ratio, R_n, quantifies the energy dissipated per loading-unloading cycle, depicting the proportion of dissipated energy relative to the total stored strain energy in each cycle. The present work includes the relationship between R_n and the normalized envelope strain at the peak of each cycle, as well as the normalized plastic strain at unloading. The results highlight the behavior of the R_n ratio. The findings indicate that all three grades of HPC investigated exhibit similar energy dissipation patterns. The plotted data reveal a bilinear behavior, characterized by an initial high rate of increase in R_n followed by a relatively slower rate of increase. Additionally, simple empirical relationships based on the observed data are also proposed. The results of this study can aid in determining elastic limits and damage indicators for HPC under repeated loading, enabling engineers to predict material behavior and optimize the design and maintenance of HPC structures in seismic and cyclic loading conditions. The results can be used for designing HPC structures capable of withstanding seismic and repeated loading conditions, enhancing their resilience and safety.

Keywords: energy dissipation, ductility, strain envelop, inelastic deformation, toughness

Notation used

σ = Normalised stress-ratio, f/fm
f = Stress
e = Strain
a_0, a_1, b_1, a_2, b_2, α_1, β_1, w = Equation constants
e_E = Normalized envelope strain
e_r = Plastic strain ratio
e_m = Strain corresponding to peak stress
f_m = failure (peak) stress
I_n = Natural logarithm
R_n = Energy dissipation ratio

1. Introduction

High-performance concrete (HPC) is a material widely acknowledged for its exceptional mechanical properties, including high compressive strength and enhanced durability (Aïtcin 1998). However, a common perception exists that materials with higher strength tend to exhibit reduced toughness compared to those with lower strength (Momin et al. 2022, C. Xie et al. 2021). Sufficient ductility in structural elements is crucial in regions prone to seismic activity, as it holds equal significance to enhancing compressive strength in constructing earthquake-resistant structures (Fitwi 2023). During severe seismic events, structures experience only a limited number of load reversals that push them into the inelastic range (Civjan & Singh 2003, Fajfar et al. 1992). The ability to dissipate energy during inelastic deformation becomes a critical factor in assessing the performance of reinforced concrete structures or structural components exposed to intense seismic actions. The energy-dissipation capacity has gained significant importance as a crucial metric to assess a member's ability to resist repeated inelastic loadings or serve as an indicator of damage (Ellingwood 2001, Ghobarah

et al. 1999, Haryanto et al. 2022, Hwang & Scribner 1984, Tafsirojjaman et al. 2019). For example, in the case of brick masonry piers subjected to lateral in-plane repeated loadings, researchers have expressed the energy dissipated per cycle of loading as a dimensionless energy dissipation ratio (Magenes & Calvi 1997, Malomo & DeJong 2021, Malomo et al. 2019). This ratio measures the dissipated energy in relation to the total stored strain energy per cycle. The concept of energy-dissipation capacity has also found extensive application in the evaluation of reinforced concrete members (Dabbaghi et al. 2022, Park & Eom 2004, Wang et al. 2020, Wu et al. 2021). Researchers have utilized indices such as the energy dissipation index (Ingham et al. 2002, Nmai & Darwin 1984), that normalizes the total dissipated energy concerning the energy stored at yield point, to characterize the cyclic performance of reinforced concrete beam. Lower energy dissipation is indicative of brittle behavior, while high-energy dissipation signifies ductile behavior.

The emergence of HPC has marked a significant breakthrough in the realm of cementitious materials over the past three decades (Xu et al. 2023). The use of higher pozzolanic materials in HPC has improved rheological behavior, characterized by enhanced flow and deformation characteristics under various loading conditions, particularly with the incorporation of materials such as ultrafine slag powder, limestone, nano clay, etc. (Arunothayan et al. 2023, Luan et al. 2023). Recent research underscores the immense potential of HPC in various engineering applications, including bridges (Saidin et al. 2023), wind tower constructions (Harte & Van Zijl 2007), and infrastructure repair (Wang et al. 2024). Structures in these applications are subjected to cyclic loadings throughout their operational lifespan, enduring millions of cycles before exhibiting signs of failure or necessitating maintenance. Cyclic loading, induced by factors such as traffic, wind, wave action, and machine vibrations (Lee & Barr 2004), contributes to the initiation and development of microcracks within the concrete matrix, leading to a gradual loss of mechanical performance (Larosche 2009). In HPC fatigue, a process characterized by mechanical weakening until eventual failure (Becks & Classen 2021, Mínguez et al. 2019, Schäfer et al. 2019, Smarzewski 2018, Sun et al. 2018, Zhang & Zhou 2022), the cyclic and repetitive loads play a pivotal role in developing microcracks within the concrete matrix, resulting in the dissipation of energy and the loss of mechanical performance (Klingbeil 2003). This intricate interplay between the exceptional properties of HPC and the challenges posed by cyclic loading forms the basis for the present work, i.e., energy dissipation characteristics of HPC under various cyclic loadings. Understanding how HPC dissipates energy in response to cyclic loading is crucial for optimizing its performance in structures subjected to repetitive stress, ultimately contributes to the advancement of resilient and durable infrastructure. Despite considerable research on energy dissipation characteristics in conventional concrete under repeated loading, studies focusing on High-Performance Concrete (HPC) remain scarce, particularly regarding its response to uniaxial repeated compressive loading. While previous research has examined the energy dissipation capacity of concrete subjected to cyclic loading (Rajput & Iqbal 2017b), the unique mechanical properties of HPC, such as its enhanced strength and durability, necessitate a focused investigation of its performance under repeated loading conditions. Some studies have studied energy dissipation in HPC for seismic applications and dynamic loading conditions (Rajput & Iqbal 2017a, Rajput et al. 2018), but there remains a gap in understanding how HPC, particularly of different grades, behaves under uniaxial repeated compressive loading.

The present work aims to study the effect of repeated compressive loading on the strength and energy dissipation characteristics of high-performance concrete. Three different grades of HPC, denoted as M_1, M_2, and M_3, with respective 28-day cube compressive strength of 65, 85, and 102 MPa, were chosen as the subjects of this investigation. The energy dissipation capacity of HPC under uniaxial compressive loading can be examined by examining the stress-strain hysteresis during repeated loading. This study aims to investigate the relationship between the dimensionless energy-dissipation ratio, R_n, and normalized envelope-strain at peak of loading cycles and the normalized plastic strains at un-loading. Additionally, empirical relationships are proposed based on the observed data to provide further understandings into energy dissipation behavior of HPC under repeated loading.

While significant research has been conducted on the energy dissipation characteristics of conventional concrete under repeated loading, studies on HPC remain limited, particularly regarding its response to uniaxial repeated compressive loading. The purpose of this investigation is to improve our understanding of energy-dissipation characteristics of HPC under cyclic compressive loadings and to formulate simple empirical relations to simulate the behavior. This study addresses this gap by examining the bilinear relationship between the energy-dissipation ratio (R_n) and strain parameters, proposing empirical relationships that can identify critical points such as elastic limits and damage initiation for different grades of HPC. The empirical relations proposed would help in comparing the performance of different grades of HPC under repeated compressive loading.

The structure of this paper is organized as follows: Section 2 provides a detailed description of the experimental methodology, including the materials used, mix designs, and testing procedures for assessing the energy dissipation characteristics of high-performance concrete (HPC) under uniaxial repeated compressive loading. Section 3 presents the results and discussion, where the stress-strain hysteresis behavior and energy dissipation ratios (R_n) for the three grades of concrete (M_1, M_2, and M_3) are analyzed and compared. The empirical relationships derived from the experimental data are also discussed in this section. Finally, Section 4 concludes the paper by summarizing the key findings.

2. Experimental Investigation

High-performance concrete (HPC) is produced by a precise selection of its constituent materials. In this study, commercially available ordinary Portland cement of 53-grade, adhering to IS: 12269 (IS 12269 2003), served as the foundation for the investigation. To achieve the desired concrete strengths, crushed basalt stone aggregates (CA) were employed, with a maximum size of 20 mm for producing M_1 mix and 12 mm down for M_2 and M_3 mixes, respectively. The locally sourced sand, meeting the grading zone-II specifications outlined in IS 383-2016 (No 1992), was used in the concrete mix as fine aggregate (FA). The concrete mix design for 3 mixes was developed following the methodology proposed by(Aïtcin 1998, Caldarone 2008), with specific details given in Table 1.

The specimens used in this research are cylindrical, with a diameter of 150 mm and a height of 400 mm, featuring flared ends. These cylindrical specimens featured flared ends, which ensured uniform loading and reduced the likelihood of localized stress concentrations. The materials utilized in the mixes included fly ash, silica fume (SF), and a water-binder (W/B) ratio of 0.3. Additionally, a superplasticizer was incorporated into the mix to improve the workability and flowability. Table 2 shows the properties of M_1, M_2, and M_3 mixes.

Table 1. Mix design details

Designation	M_1	M_2	M_3
W/B ratio	0.34	0.28	0.25
Cement, kg/m^3	376	420	480
FA, kg/m^3	702	660	672
CA, kg/m^3	1125	1125	1125
Fly ash, kg/m^3	90	70	60
SF, kg/m^3	–	40	50
Superplasticizer – Glenium B233 in %	0.38	0.5	0.7

Table 2. Properties of HPC

Grade	Compressive Strength (MPa)	Axial Deformation (mm)	Poisson's Ratio	Modulus of Elasticity (MPa)
M1	65	0.0025	0.168	45813
M2	85	0.0032	0.153	48559
M3	102	0.0038	0.131	48973

Specimens were instrumented to measure the axial displacements at two locations diagonally opposite to each other. Linear variable displacement transducers (LVDTs) were used to sensor the displacements along a fixed gauge length of 200 mm. Curved brackets were fixed to the surface of specimens using epoxy. LVDTs had a total stroke length of 2.5 mm and an output of 10 volts at the full displacement. The specimens were subjected to repeated compressive loading through a carefully controlled and systematic process. A servo-hydraulic testing machine was employed to apply the compressive loads. The servo-hydraulic testing machine used for testing the specimens had a capacity of 3000 kN and a loading rate of 10 N/Sec. To avoid the frictional resistance between the specimens and platens, two Teflon sheets were placed at the top and bottom. The specimens were securely positioned within the loading frame, and a uniaxial compressive load was then steadily and repeatedly applied. The loading process involved a cyclic pattern, wherein the specimens experienced a sequence of compressive loading and unloading cycles. Each loading cycle was meticulously controlled, ensuring uniformity and reproducibility. The loading mechanism simulated realistic conditions, mimicking the cyclic loading scenarios that structural elements often encounter during seismic events or other dynamic forces.

This rigorous loading approach allowed for a comprehensive examination of the energy-dissipation characteristics of the HPC under consideration. The detailed loading protocol adhered to the standards and guidelines commonly accepted in structural testing, providing a reliable and controlled environment for assessing the specimens' response to cyclic compressive loadings.

In every loading cycle as depicted in Figure 1, the peak strain approximately coincided with the envelope curves. The envelope curves represent the limit of stress values in the stress-strain domain that any loading curve cannot exceed without causing apparent failure in the concrete (Karsan 1968). All stress-strain curves remained within this envelope curve, irrespective of the load pattern. The load histories in the ascending zone of the stress-strain curves were regulated by continuously observing the incremental strain during each cycle. The load was released when the loading curves tended to descend in the descending zone of stress-strain curves.

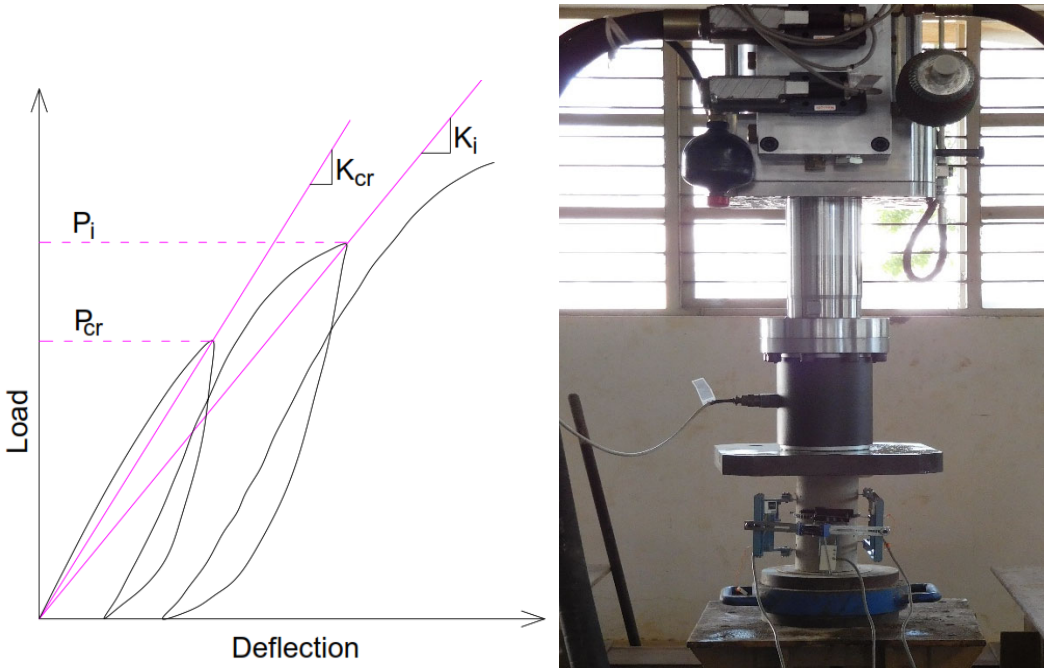

Fig. 1. Typical repeated loading test

The envelope stress-strain curve for the three grades of HPC was constructed by plotting the peak stress-strain values observed in every cycle under compressive loadings. To ensure consistency, both stress and strain were expressed in non-dimensional form. The stress coordinates were normalized relative to the failure (peak) stress, f_m, exhibited by the specimens. Similarly, the strain coordinates were normalized relative to e_m, which represents the axial strain at the point of reaching the peak stress. Figure 2 to Figure 4 presents the envelope stress-strain curves for the M_1, M_2 and M_3 grade of HPC respectively. These plots provide a comprehensive representation of the stress-strain behavior and highlight the overall trends observed in the three different grades of HPC.

Using MATLAB, an expression (Eqn. 1) was derived for the three curves corresponding to mixes M_1, M_2, and M_3 based on the test result data obtained during cyclic loading. The stress coordinates (σ) were normalized relative to the peak stresses (f_m) observed in all specimens. Simultaneously, the strain coordinates (ε) were normalized concerning the axial strains (e_m) corresponding to points of peak stress attainment. This normalization process facilitates a comparative analysis of the stress-strain behavior across different mixes, providing a standardized basis for evaluating their performance under cyclic loading conditions.

$$f(\sigma) = a_0 + a_1\cos(\epsilon_\omega) + b_1\sin(\epsilon_\omega) \tag{1}$$

Equation 1 is expressed in the form of a Fourier series, and the corresponding parameters for all the curves are presented in Table 3. I_c refers to the critical index used to indicate the initiation of significant damage or deterioration in the concrete material during repeated loading.

Table 3. Parameter details for eqn. 1

Mix	a_0	a_1	b_1	w	I_c
M_1	-0.34	0.28	1.32	1.40	0.98
M_2	0.41	-0.42	0.39	2.45	0.97
M_3	0.38	-0.36	0.52	2.21	0.98

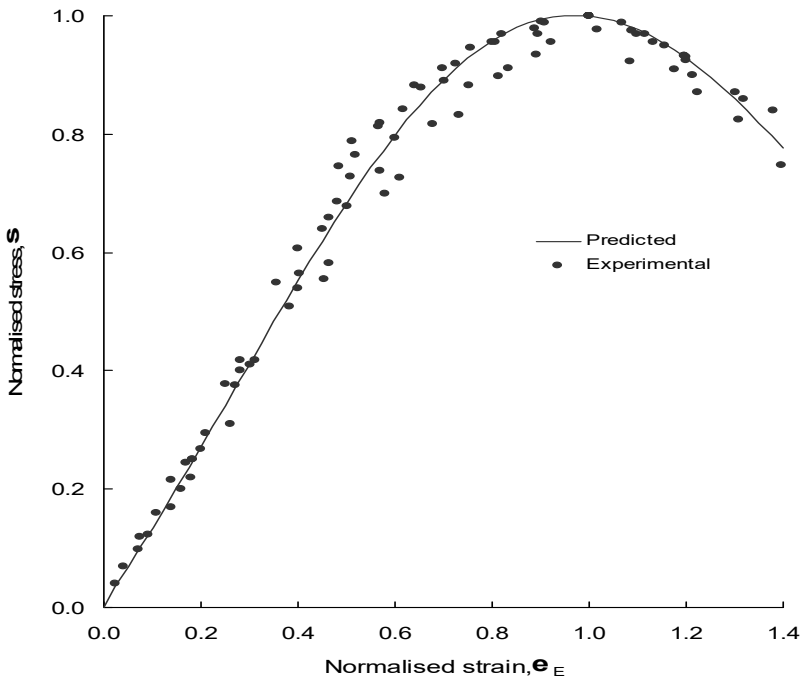

Fig. 2. Envelope stress-strain curve for M_1 concrete

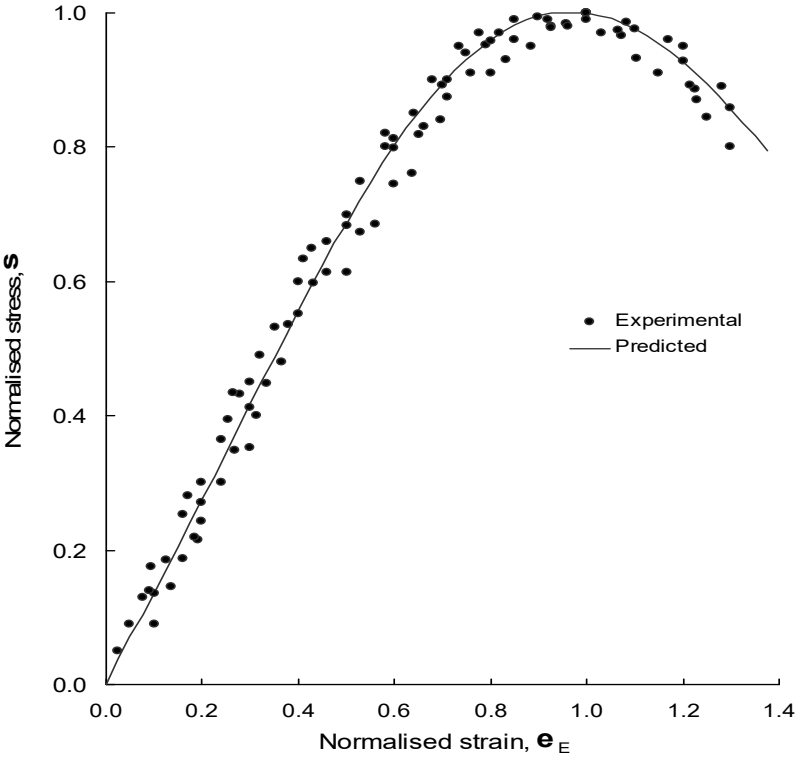

Fig. 3. Envelope stress-strain curve for M_2 concrete

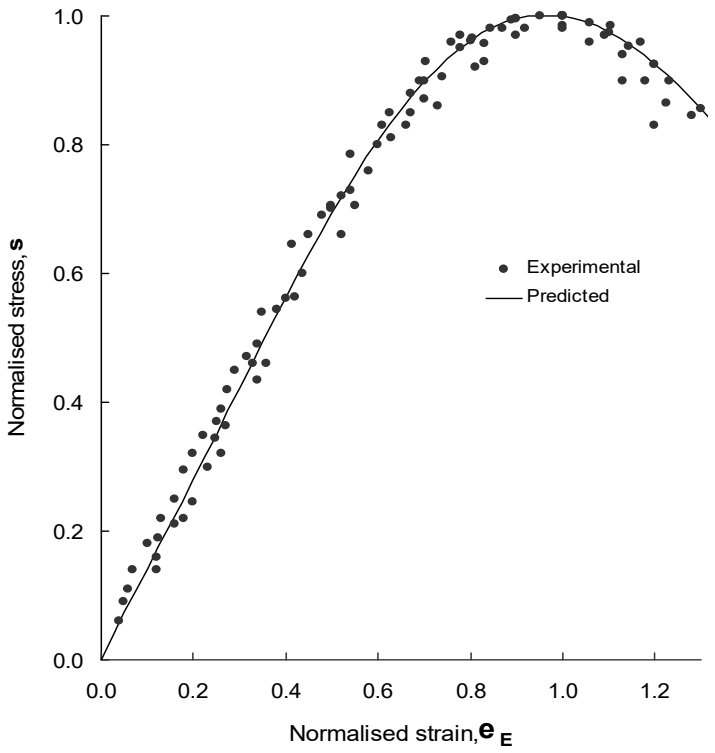

Fig. 4. Envelope stress-strain curve for M_3 concrete

3. Energy Dissipation

3.1. Energy dissipation ratio, R_n

Perhaps one of the most crucial aspects of structural performance under repeated loadings lies in the structure's capacity to efficiently dissipate energy (Golias et al. 2021, Mirzai et al. 2020). In the present investigation, the energy-dissipation ratio, R_n, is utilized to measure the energy dissipated per loading and unloading cycle. R_n is characterized as the proportion of energy dissipated per cycle relative to the total input energy (Sucuoğlu & Nurtuğ 1995), as illustrated in Figure 5, representing a typical reloading-unloading cycle. The energy dissipated per cycle corresponds to the area enclosed by the re-loading or un-loading loops specific to that cycle. Total input energy per cycle refers to total stored strain energy during the reloading-unloading process. The area under the curve was determined using a digital planimeter. For each cycle of loading and unloading, three R_n values were obtained. The mean values were plotted against the non-dimensional envelope strains at peak of every cycle and against the normalized plastic strains during un-loading.

3.2. R_n against envelope strain

Figures 6, 7, and 8 show the plots of R_n ratio vs. normalized envelope strain, e_E, for three grades of concrete tested. Based on the experimental points, using the least square method, a suitable single general empirical expression is formed (Eqn. 2) for all the three grades of concrete to fit the data best.

$$R_n = \beta_1 X\ In(\varepsilon_E{}^{\alpha_1} + 1) \tag{2}$$

The correlation index, i.e., obtained for these empirical curves, is 0.92 for M_1, 0.96 for M_2, and 0.95 for M_3 concrete. This observation suggests that each empirical curve fits well with the experimental data, indicating a favorable degree of accuracy and alignment between the predicted values and the actual measurements. The values of α_1 are 0.55, 0.53, and 0.55 for M_1, M_2, and M_3 concrete, respectively. The values of β_1 are 0.485, 0.45, and 0.48 for M_1, M_2 and M_3 grades respectively. In general, the relationship between the energy-dissipation ratio, R_n, and envelope strain exhibits a bilinear pattern (Caldarone 2008, Ciampi et al. 1982, Golias et al. 2021, Gong et al. 2022, Karsan 1968, Mirzai et al. 2020, Nazar & Sinha 2009, Sucuoğlu & Nurtuğ 1995, Q. Xie et al. 2021). The initial portion shows a linear increase in R_n with a high rate, accompanied by a relatively slower rate of strain increase. Subsequently, there is another linear portion with a slower rate of R_n increase, coinciding with a faster rate of strain ratio increase. (Alshebani 1999, Naraine & Sinha 1989) have made similar observations for clay brick and sandblast brick masonry, respectively. A potential limitation of

the developed equation (Eqn. 2) is its assumption of a bilinear pattern in the relationship between the energy dissipation ratio (R_n) and normalized envelope strain (e_E), which does not fully capture more intricate or non-linear behaviors that could exist in certain conditions or materials.

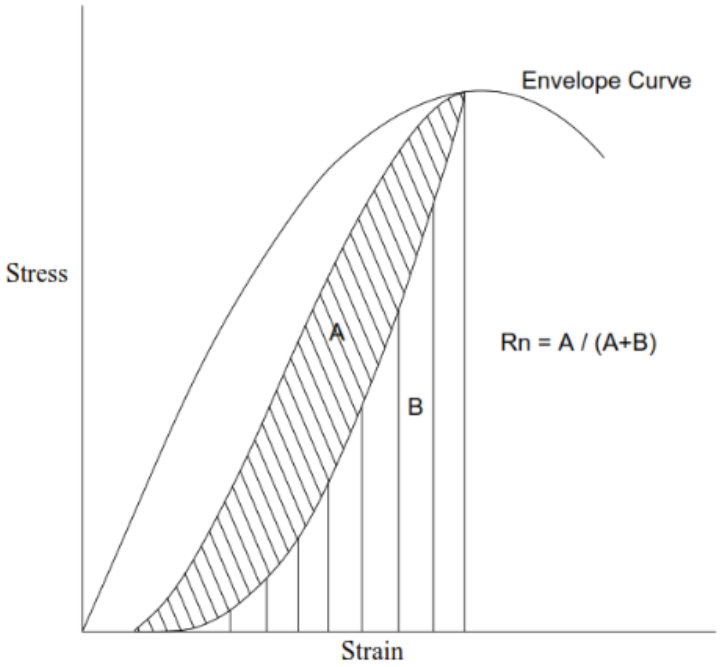

Fig. 5. Energy dissipation ratio R_n

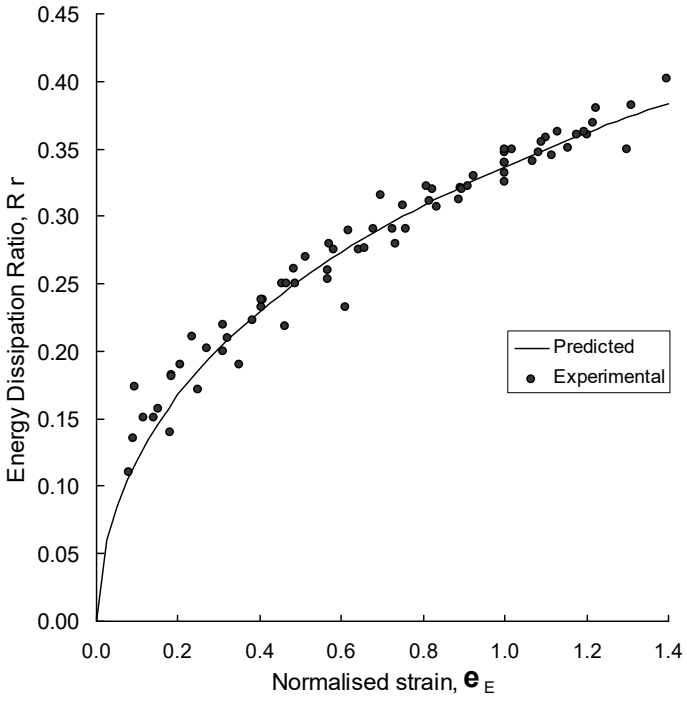

Fig. 6. R_n versus envelope strain for M_1

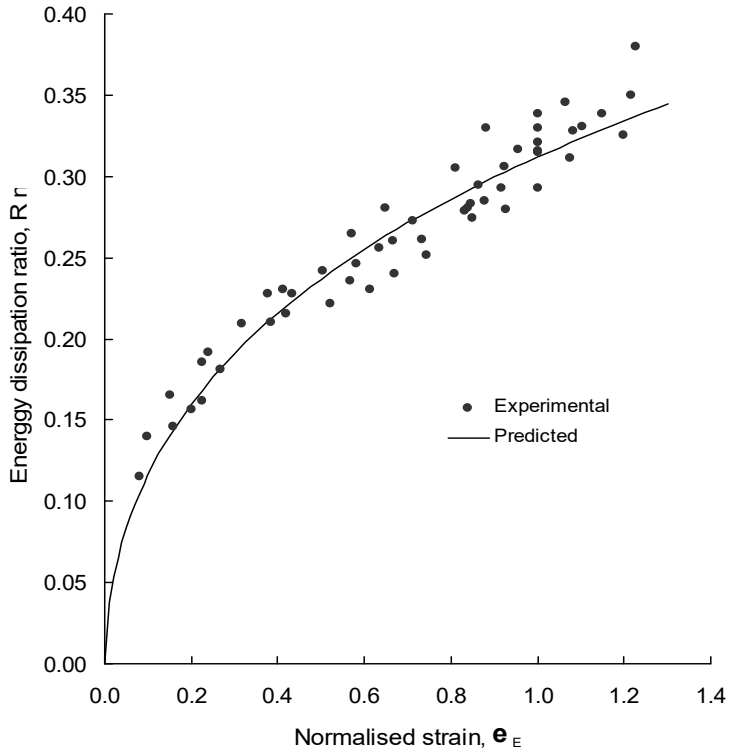

Fig. 7. R_n versus envelope strain for M_2

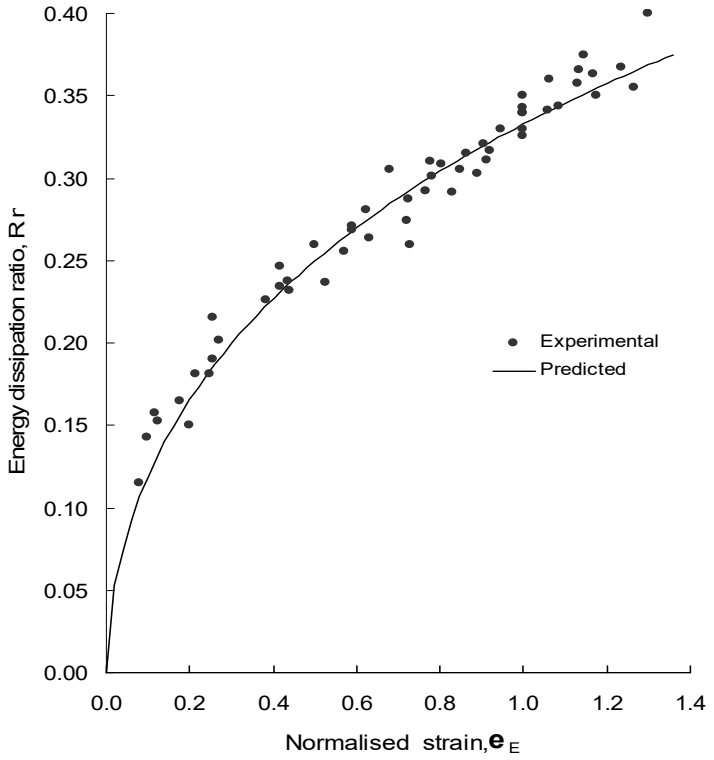

Fig. 8. R_n versus envelope strain for M_3

In the case of M_1 mix, the R_n ratio increases approximately linearly up to a value of approximately 0.2, corresponding to an envelope strain ratio of approximately 0.3, after which it again increases approximately linearly to a value of about 0.38, corresponding to an envelope strain ratio of 1.4. For M_2 concrete, the R_n ratio increases linearly up to the value of approximately 0.2, corresponding to an envelope strain ratio of 0.33, after which it again increases approximately linearly to a value of 0.35, corresponding to an envelope strain ratio of

approximately 1.3. The M_3 concrete Rn ratio increases approximately linearly to 0.21, corresponding to an envelope strain ratio of approximately 0.35. Then, it again increases approximately linearly to a value of approximately 0.36, corresponding to an envelope strain ratio of approximately 1.3.

The initial rapid increase in the R_n ratio during the early stage of repeated loadings could be attributed to the formation and growth of microcracks in the concrete. As the loading progresses, the rate of R_n increase diminishes, which is attributed to the widening of the microcracks. The initial linear portion of R_n versus envelope strain (ε_E) curves can be linked to the material's elastic response, as the formation of microcracks does not lead to a significant accumulation of plastic strains (Yuan et al. 2019). In the case of M_1 grade of concrete, the initial linear portion of the R_n curves exists up to an envelope strain ratio of around 0.3. Based on Figure 2, this envelope strain ratio corresponds to a stress ratio of 0.42. Therefore, it can be hypothesized from the energy dissipation characteristics that a stress ratio of 0.42 can be considered the elastic limit for M_1 grade of concrete. The stress-strain curve also exhibits an approximately linear behavior up to a stress ratio of 0.42 for M_1 concrete. According to the plastic strain curves of ε_r versus ε_E presented in (Yuan et al. 2019), unloading from an envelope strain ratio of 0.3 results in a plastic strain ratio of 0.003. The extremely low value of plastic strain confirms the material's approximate elastic response.

Similarly, for M_2 and M_3 concrete, the initial linear portion of the R_n curves exists up to an envelope strain ratio of approximately 0.33 and 0.35, respectively. From the envelope stress-strain curves (Figures 4 and 5), these values correspond to stress ratios of 0.46 and 0.5 for M_2 and M_3 concrete, respectively, which can be taken as their elastic limits. The envelope stress-strain curves are also observed to be linear up to these stress values. According to the plastic strain curves of plastic strain ε_r versus envelope strain ε_E presented in (Khadiranaikar 2003), un-loading from an envelope strain ratio of 0.33 and 0.35 results in a plastic strain of approximately 0.0025 and 0.002 for M_2 and M_3 concrete, respectively. Such small plastic strain ratio values support the elastic limit hypothesis.

3.3. R_n against plastic strain

The energy dissipation ratio R_n versus the non-dimensional plastic strain at unloading, ε_r, for all three grades of concrete investigated, are plotted in Figures 9, 10, and 11. A similar empirical relationship was developed, which is given in Eqn. 3.

$$R_n = \frac{1}{\beta_2}\varepsilon_r{}^{\alpha_2} XIn(\varepsilon_r{}^{\alpha_2} + 1.2) \tag{3}$$

The correlation index obtained for these empirical curves is 0.95, 0.92, and 0.94 for M_1, M_2, and M_3 grades of concrete, respectively. This indicates a good fit of the empirical curves to the experimental data. The values of the constants α_1 and β_1) were obtained from the test data analysis. The values of α_1 are 0.113, 0.1, and 0.113 for M_1, M_2, and M_3 concrete, respectively. The values of β_1 are 1.781, 1.65, and 1.54 for M_1, M_2, and M_3 concrete, respectively.

The R_n versus e_r curves also exhibit an approximate bilinear nature, similar to the R_n versus e_E curves. The initial rapid increase in the R_n ratio during the early stage of repeated loadings is attributed to the development of microcracks, which do not lead to significant accumulation of plastic strains. However, as the microcracks widen, substantial plastic strain is developed, resulting in a low R_n ratio increase rate. For M_1 concrete, the point at which the R_n versus e_r curve deviates from the initial linear portion occurs at a value of e_r (plastic strain) of nearly 0.03. The point where non-linearity in plastic strain begins can be interpreted as the point in the loading history denoting the beginning of the deterioration of the microcracks in the material. Based on the empirical plastic strain curve presented in (Milad 1999), the values of e_r of 0.03 for M_1 concrete correspond to a value of e_E of approximately 0.55, and the latter corresponds to an envelope stress ratio of 0.74 (Figure 2). Similarly, for M_2 concrete, the value of e_r of 0.015 corresponds to a value of e_E of approximately 0.55, and the latter corresponds to an envelope stress ratio of 0.75 (Figure 3). For M_3 concrete, non-linearity begins at e_r of 0.0135, which corresponds to an envelope strain ratio e_E of approximately 0.56, which corresponds to an envelope stress ratio of 0.76. Consequently, based on the energy-dissipation characteristics, it is postulated that the stress ratios can serve as reliable damage indicators for the corresponding grades of concrete.

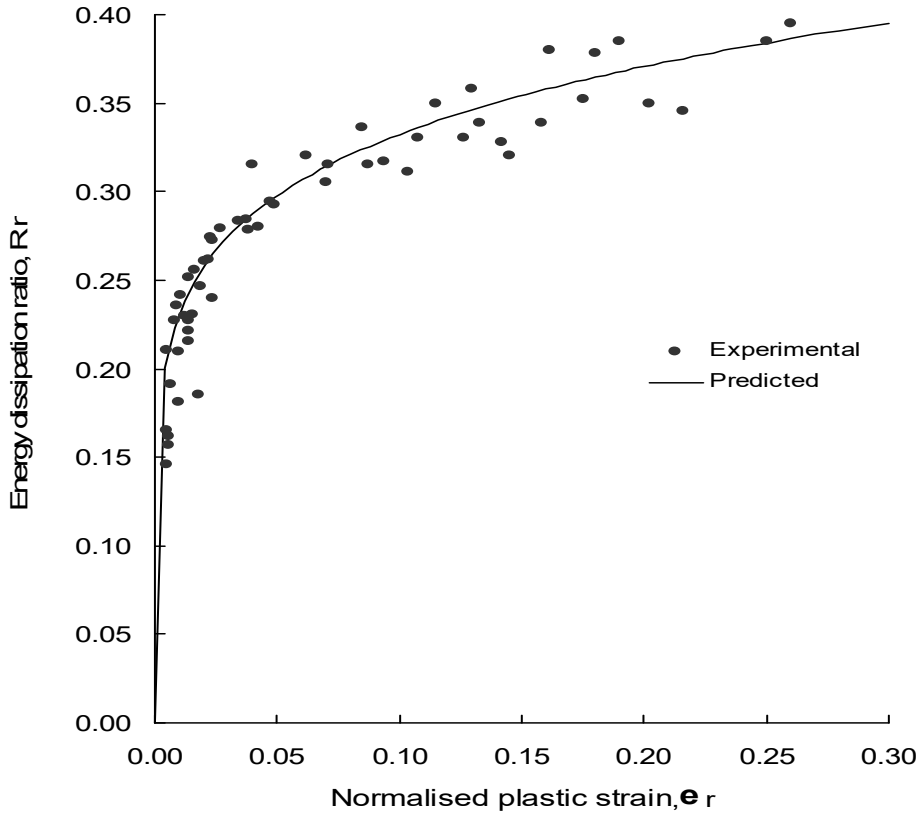

Fig. 9. R_n versus plastic strain for M_1 concrete

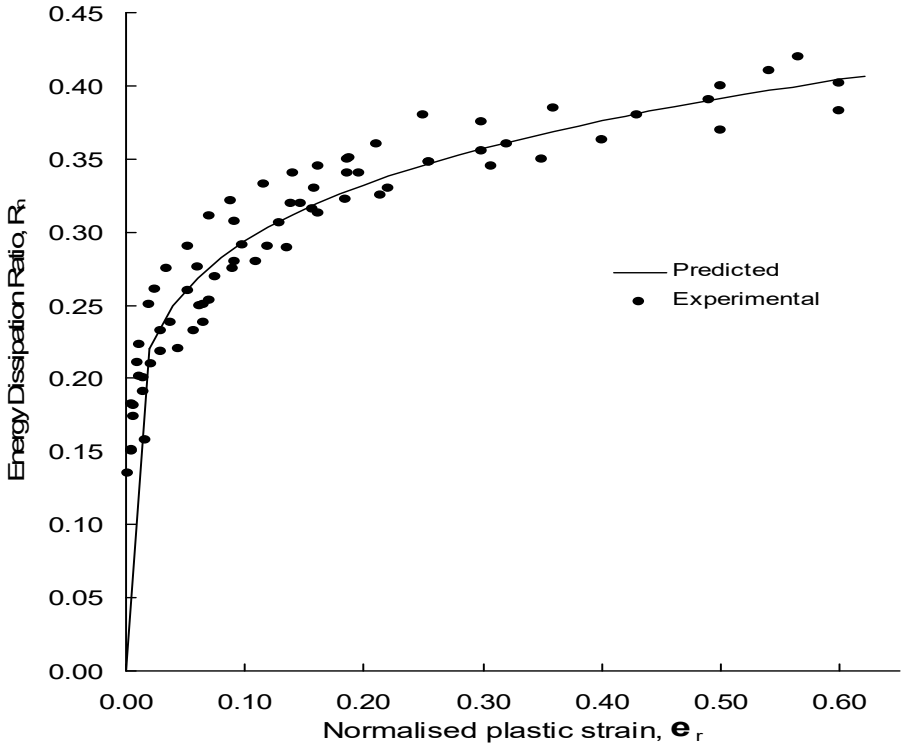

Fig.10. R_n versus plastic strain for M_2 concrete

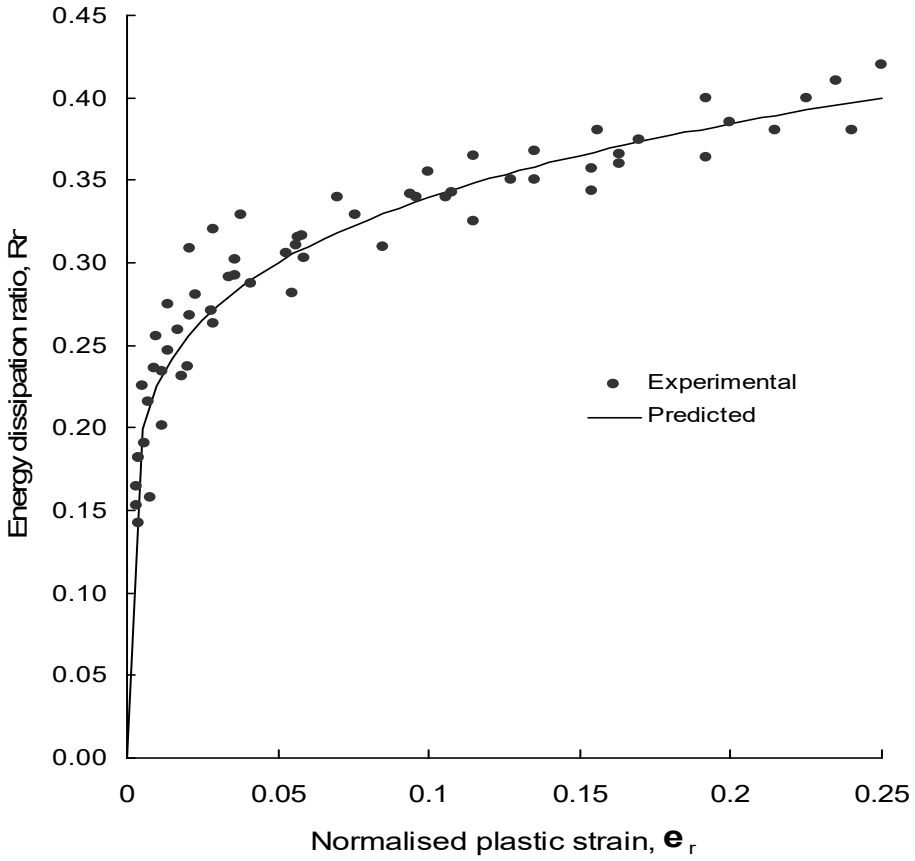

Fig. 11. R_n versus plastic strain for M_3 concrete

3.4. Discussions

The results of this study align with observations made in related research (Khadiranaikar 2003, Park & Eom 2004, Wang et al. 2020). The bilinear nature of the relationship between the energy-dissipation ratio (R_n) and both envelope strain (e_E) and plastic strain (ε_r) is consistent with prior studies (Khadiranaikar 2003, Li et al. 2024, Naraine & Sinha 1989, Yuan et al. 2019). The initial linear increase in R_n, attributed to microcrack formation and subsequent slower rates, is a pattern noted in clay brick masonry (Naraine & Sinha 1989) and sand-plast brick masonry (Yuan et al. 2019). The experimental data presented for the strain energy stored indicates an increasing trend with the strain and is similar to the stress-strain curve, indicating a fundamental correspondence between strain energy and the stress-strain curve. Damage occurring in the concrete has been characterized by cumulative damage and damping energy. Damage is progressive and characterized at very low strain levels. In the initial stages, damage was more in lower-strength specimens and less in higher-strength specimens. However, the trend changed and reversed near the peak strain, where damage is greater for higher-strength specimens. There was a progressive increase of damping energy with the strain. Higher energy dissipation was observed when damping higher-strength specimens.

The empirical expressions proposed in this study for R_n against envelope and plastic strain exhibit favorable correlations, indicating good alignment with experimental data. However, these correlations should be interpreted considering potential variations in concrete mixtures, loading conditions, and specimen geometries. The empirical expressions assume a bilinear pattern in the relationship between R_n and envelope/plastic strain. This assumption oversimplifies the complexity of certain conditions or materials that exhibit more intricate or non-linear behaviors. The study focuses on three grades of concrete (M_1, M_2, M_3), and the proposed relationships will not be generalized well to different concrete mixtures with distinct material properties. The findings from this study have significant field applications, particularly in the design and evaluation of structures subjected to cyclic or dynamic loading, such as bridges, pavements, and buildings in seismic zones. The identified energy dissipation characteristics and damage indicators, including the elastic limits and non-linear transitions in R_n values, provide information for engineers to optimize concrete performance under repeated loading conditions. These results can be integrated into seismic design codes to improve the safety and durability of infrastructure, assist in designing pavements resistant to wear and cracking, and enable more reliable health monitoring of bridges.

4. Summary and Conclusions

In this investigation, the energy-dissipation characteristics of HPC under uniaxial repeated compressive loading are examined. The stress-strain hysteresis of the repeated loading was used to assess the energy-dissipation capacity of HPC, and it was quantified through the dimensionless energy dissipation ratio, R_n. The R_n values are plotted against the normalized envelope strain and the normalized plastic strain for the three grades of concrete studied. Simple empirical relationships were proposed for these plots. The plots depicting the R_n ratio against both envelope and plastic strain exhibited a bilinear nature, with an initial linear high rate of increase in R_n, followed by a relatively slower linear rate of increase in R_n, alongside a higher increase in strain. The initial linear portion of the R_n versus envelope strain curves was associated with the material's elastic response. Based on these R_n curves, it is hypothesized that a stress level of $0.42f_m$, $0.46f_m$, and $0.5f_m$ can serve as the elastic limits for M_1, M_2, and M_3 concrete, respectively. Moreover, the relationship between R_n and e_r can be employed to identify the initiation of the strength deterioration process. The normalized stress levels of 0.74, 0.75, and 0.76, corresponding to the points where the R_n versus e_r curve deviates from the initial linear portion, can be hypothesized as the damage indicators for M_1, M_2, and M_3 concrete, respectively.

Although the three grades of concrete exhibited similar energy dissipation behavior, this similarity can be attributed to the comparable mix designs and the similar composition of materials (such as fly ash, silica fume, and basalt aggregates) used in all three grades. The results suggest that, under repeated compressive loading, energy dissipation characteristics may be influenced more by the material composition and the loading conditions than by the strength of the concrete alone. This finding highlights that energy dissipation can be a consistent indicator of concrete performance across different HPC grades and can be applied to evaluating the behavior of HPC in structures subjected to cyclic loading. This research provides a basis for future investigations to investigate more intricate non-linear behaviors and additional influencing factors in high-performance concrete's cyclic response while encouraging practical applications of the developed empirical relationships in the design and evaluation of structures subjected to repeated loading. While the results of this study are valuable for understanding the energy dissipation capacity of HPC under cyclic loading, they may not fully represent the response of concrete structures under actual seismic conditions. Future research could aim to investigate the effects of higher strain rates or dynamic loading on HPC to simulate realistic seismic behavior better.

The authors extend their appreciation to the Deanship of Research and Graduate Studies at King Khalid University for funding this work through Large Research Project under grant number RGP2/305/45.

References

Aïtcin, P.-C. (1998). *High performance concrete*. CRC press. https://doi.org/10.4324/9780203475034

Alshebani, M. (1999). *Response of brick masonry under cyclic loading* Ph. D. Thesis, Indian Institute of Technology, Delhi India.

Arunothayan, A. R., Nematollahi, B., Khayat, K. H., Ramesh, A., & Sanjayan, J. G. (2023). Rheological characterization of ultra-high performance concrete for 3D printing. *Cement and Concrete Composites*, *136*, 104854.

Becks, H., & Classen, M. (2021). Mode II behavior of high-strength concrete under monotonic, cyclic and fatigue loading. *Materials*, *14*(24), 7675.

Caldarone, M. A. (2008). *High-strength concrete: a practical guide*. CRC press.

Ciampi, V., Eligehausen, R., Bertero, V. V., & Popov, E. P. (1982). *Analytical model for concrete anchorages of reinforcing bars under generalized excitations*. College of Engineering, University of California Berkeley, CA, USA.

Civjan, S. A., & Singh, P. (2003). Behavior of shear studs subjected to fully reversed cyclic loading. *Journal of Structural Engineering*, *129*(11), 1466-1474. https://doi.org/10.1061/(ASCE)0733-9445(2003)129:11(1466)

Dabbaghi, F., Yang, T., Tanhadoust, A., Emadi, S., Dehestani, M., & Yousefpour, H. (2022). Experimental and numerical investigation on post-fire seismic performance of light weight aggregate reinforced concrete beams. *Engineering Structures*, *268*, 114791. https://doi.org/10.1016/j.engstruct.2022.114791

Ellingwood, B. R. (2001). Earthquake risk assessment of building structures. *Reliability Engineering & System Safety*, *74*(3), 251-262. https://doi.org/10.1016/S0951-8320(01)00105-3

Fajfar, P., Vidic, T., & Fischinger, M. (1992). On energy demand and supply in SDOF systems. In *Non-linear seismic analysis and design of reinforced concrete buildings* (pp. 49-70). CRC Press.

Fitwi, T. H. (2023). *Earthquakes, Reinforced Concrete Structures, and Circular Economy: A Systematic Review of Studies*. Proceedings of The 17th East Asian-Pacific Conference on Structural Engineering and Construction, 2022: EASEC-17, Singapore, https://doi.org/10.1007/978-981-19-7331-4_86

Ghobarah, A., Abou-Elfath, H., & Biddah, A. (1999). Response-based damage assessment of structures. *Earthquake engineering & structural dynamics*, *28*(1), 79-104. https://doi.org/10.1002/(SICI)1096-9845(199901)28:1<79::AID-EQE805>3.0.CO;2-J

Golias, E., Zapris, A. G., Kytinou, V. K., Osman, M., Koumtzis, M., Siapera, D., Chalioris, C. E., & Karayannis, C. G. (2021). Application of X-shaped CFRP ropes for structural upgrading of reinforced concrete beam–column joints under cyclic loading–experimental study. *Fibers*, *9*(7), 42. https://doi.org/10.3390/fib9070042

Gong, F., Shi, R., & Xu, L. (2022). Linear energy storage and dissipation laws of concrete under uniaxial compression at different ages. *Construction and Building Materials*, *318*, 125963. https://doi.org/10.1016/j.conbuildmat.2021.125963

Harte, R., & Van Zijl, G. P. (2007). Structural stability of concrete wind turbines and solar chimney towers exposed to dynamic wind action. *Journal of Wind engineering and industrial aerodynamics*, *95*(9-11), 1079-1096. https://doi.org/10.1016/j.jweia.2007.01.028

Haryanto, Y., Hsiao, F.-P., Hu, H.-T., Han, A. L., Chua, A. W., Salim, F., & Nugroho, L. (2022). Structural behavior of negative moment region NSM-CFRP strengthened RC T-beams with various embedment depth under monotonic and cyclic loading. *Composite Structures*, *301*, 116214. https://doi.org/10.1016/j.compstruct.2022.116214

Hwang, T.-H., & Scribner, C. F. (1984). R/C member cyclic response during various loadings. *Journal of Structural Engineering*, *110*(3), 477-489. https://doi.org/10.1061/(ASCE)0733-9445(1984)110:3(477)

Ingham, J., Liddell, D., & Davidson, B. (2002). An assessment of parameters describing the response of a reinforced concrete beam. *Bulletin of the New Zealand Society for Earthquake Engineering*, *35*(1), 1-16.

IS12269, I. S. D. (2003). Specification for 53 grade ordinary Portland cement. *Bureau of Indian Standards, New Delhi*.

Karsan, D. I. (1968). *Behavior of plain concrete under variable load histories*. Rice University.

Khadiranaikar, R. (2003). *Experimental investigation of high performance concrete under repeated compressive loading* IIT Delhi.

Klingbeil, N. W. (2003). A total dissipated energy theory of fatigue crack growth in ductile solids. *International Journal of Fatigue*, *25*(2), 117-128. https://doi.org/10.1016/S0142-1123(02)00073-7

Larosche, C. (2009). Types and causes of cracking in concrete structures. In *Failure, distress and repair of concrete structures* (pp. 57-83). Elsevier. https://doi.org/10.1533/9781845697037.1.57

Lee, M., & Barr, B. (2004). An overview of the fatigue behaviour of plain and fibre reinforced concrete. *Cement and Concrete Composites*, *26*(4), 299-305. https://doi.org/10.1016/S0958-9465(02)00139-7

Li, K.-S., Yao, S.-L., Cheng, L.-Y., Wang, R.-Z., Sun, L., Gu, H.-H., Wang, J., Lu, T.-W., Zhang, C.-C., & Zhang, X.-C. (2024). Creep-fatigue life prediction of notched structure after an advanced surface strengthening treatment in a nickel-based superalloy at 650° C. *International Journal of Plasticity*, *173*, 103861. https://doi.org/10.1016/j.ijplas.2023.103861

Luan, C., Yang, Q., Lin, X., Gao, X., Cheng, H., Huang, Y., Du, P., Zhou, Z., & Wang, J. (2023). The Synergistic Effects of Ultrafine Slag Powder and Limestone on the Rheology Behavior, Microstructure, and Fractal Features of Ultra-High Performance Concrete (UHPC). *Materials*, *16*(6), 2281. https://doi.org/10.3390/ma16062281

Magenes, G., & Calvi, G. M. (1997). In-plane seismic response of brick masonry walls. *Earthquake engineering & structural dynamics*, *26*(11), 1091-1112. https://doi.org/10.1002/(SICI)1096-9845(199711)26:11<1091::AID-EQE693>3.0.CO;2-6

Malomo, D., & DeJong, M. J. (2021). A Macro-Distinct Element Model (M-DEM) for simulating the in-plane cyclic behavior of URM structures. *Engineering Structures*, *227*, 111428. https://doi.org/10.1016/j.engstruct.2020.111428

Malomo, D., DeJong, M. J., & Penna, A. (2019). Distinct element modelling of the in-plane cyclic response of URM walls subjected to shear-compression. *Earthquake engineering & structural dynamics*, *48*(12), 1322-1344. https://doi.org/10.1002/eqe.3178

Mínguez, J., Gutiérrez, L., González, D. C., & Vicente, M. A. (2019). Plain and fiber-reinforced concrete subjected to cyclic compressive loading: study of the mechanical response and correlations with microstructure using CT scanning. *Applied Sciences*, *9*(15), 3030. https://doi.org/10.3390/app9153030

Mirzai, N. M., Attarnejad, R., & Hu, J. W. (2020). Analytical investigation of the behavior of a new smart recentering shear damper under cyclic loading. *Journal of Intelligent Material Systems and Structures*, *31*(4), 550-569. https://doi.org/10.1177/1045389X19888786

Momin, A. I. A., Khadiranaikar, R., & Zende, A. A. (2022). Modulus of Elasticity of High-Performance Concrete Beams Under Flexure-Experimental Approach. In *Recent Trends in Construction Technology and Management: Select Proceedings of ACTM 2021* (pp. 57-69). Springer. https://link.springer.com/chapter/10.1007/978-981-19-2145-2_5

Naraine, K., & Sinha, S. (1989). Energy Dissipation in Brick Masonry under Cyclic compressive Loading. Masonry (4). Proc. 2 nd Int. Masonry Conf. London,

Nazar, M. E., & Sinha, S. (2009). *Energy Dissipation Characteristics of Interlocking Grouted Brick Masonry*. 11 th Canadian Masonry Symposium.

Nmai, C. K., & Darwin, D. (1984). *Cyclic behavior of lightly reinforced concrete beams*.

No, A. (1992). Specification for aggregates from natural sources for concrete. *Bs*, *882*(1992), 1-14.

Park, H., & Eom, T. (2004). *Energy dissipation capacity of reinforced concrete members*. CTBUH 2004 Seoul conference,

Rajput, A., & Iqbal, M. A. (2017a). Ballistic performance of plain, reinforced and pre-stressed concrete slabs under normal impact by an ogival-nosed projectile. *International journal of impact engineering*, *110*, 57-71. https://doi.org/10.1016/j.ijimpeng.2017.03.008

Rajput, A., & Iqbal, M. A. (2017b). Impact behavior of plain, reinforced and prestressed concrete targets. *Materials & Design*, *114*, 459-474.

Rajput, A., Iqbal, M. A., & Gupta, N. (2018). Ballistic performances of concrete targets subjected to long projectile impact. *Thin-Walled Structures*, *126*, 171-181. https://doi.org/10.1016/j.tws.2017.01.021

Saidin, S. S., Kudus, S. A., Jamadin, A., Anuar, M. A., Amin, N. M., Ya, A. B. Z., & Sugiura, K. (2023). Vibration-based approach for structural health monitoring of ultra-high-performance concrete bridge. *Case Studies in Construction Materials*, *18*, e01752. https://doi.org/10.1016/j.cscm.2022.e01752

Schäfer, N., Gudžulić, V., Timothy, J. J., Breitenbücher, R., & Meschke, G. (2019). Fatigue behavior of HPC and FRC under cyclic tensile loading: Experiments and modeling. *Structural Concrete*, *20*(4), 1265-1278. https://doi.org/10.1002/suco.201900056

Smarzewski, P. (2018). Analysis of failure mechanics in hybrid fibre-reinforced high-performance concrete deep beams with and without openings. *Materials*, *12*(1), 101. https://doi.org/10.3390/ma12010101

Sucuoğlu, H., & Nurtuğ, A. (1995). Earthquake ground motion characteristics and seismic energy dissipation. *Earthquake engineering & structural dynamics*, *24*(9), 1195-1213. https://doi.org/10.1002/eqe.4290240903

Sun, Q., Meng, Z., Zhou, G., Lin, S.-P., Kang, H., Keten, S., Guo, H., & Su, X. (2018). Multi-scale computational analysis of unidirectional carbon fiber reinforced polymer composites under various loading conditions. *Composite Structures*, *196*, 30-43. https://doi.org/10.1016/j.compstruct.2018.05.025

Tafsirojjaman, T., Fawzia, S., Thambiratnam, D., & Zhao, X.-L. (2019). Behaviour of CFRP strengthened CHS members under monotonic and cyclic loading. *Composite Structures*, *220*, 592-601. https://doi.org/10.1016/j.compstruct.2019.04.029

Wang, S., Liu, S., Zhang, W., & Guo, B. (2024). Research on improving the durability performance of damaged concrete based on ultra high performance concrete repair. *Engineering Reports*, *6*(6), e12780. https://doi.org/10.1002/eng2.12780

Wang, Y., Liu, Z., Yang, W., Hu, Y., & Chen, Y. (2020). Damage index of reinforced concrete members based on the energy dissipation capability degradation. *The Structural Design of Tall and Special Buildings*, *29*(2), e1695. https://doi.org/10.1002/tal.1695

Wu, K., Chen, F., Lin, J., Zhao, J., & Zheng, H. (2021). Experimental study on the interfacial bond strength and energy dissipation capacity of steel and steel fibre reinforced concrete (SSFRC) structures. *Engineering Structures*, *235*, 112094. https://doi.org/10.1016/j.engstruct.2021.112094

Xie, C., Cao, M., Khan, M., Yin, H., & Guan, J. (2021). Review on different testing methods and factors affecting fracture properties of fiber reinforced cementitious composites. *Construction and Building Materials*, *273*, 121766. https://doi.org/10.1080/15583058.2019.1674943

Xie, Q., Xu, D., Wang, Y., Zhang, L., & Xin, R. (2021). Seismic behavior of brick masonry walls representative of ancient Chinese pagoda walls subjected to in-plane cyclic loading. *International Journal of Architectural Heritage*, *15*(9), 1336-1348. doi.org/10.1080/15583058.2019.1674943

Xu, L., Yao, Y., Li, Y., Su, J., & Wu, Y. (2023). Review of the Interfacial Bonding Properties between Ultrahigh-Performance Concrete and Normal Concrete. *Applied Sciences*, *13*(11), 6697. https://doi.org/10.3390/app13116697

Yuan, J., Chen, X., & Guo, S. (2019). Experimental study on cyclic tensile behaviour of air-entrained concrete after frost damage. *Sādhanā*, *44*(8), 189. https://link.springer.com/article/10.1007/s12046-019-1172-3

Zhang, J.-Z., & Zhou, X.-P. (2022). Fracture process zone (FPZ) in quasi-brittle materials: Review and new insights from flawed granite subjected to uniaxial stress. *Engineering Fracture Mechanics*, *274*, 108795. https://doi.org/10.1016/j.engfracmech.2022.108795